



Article

GDP Forecasting Model for China's Provinces Using Nighttime Light Remote Sensing Data

Yan Gu ¹, Zhenfeng Shao ^{1,*}, Xiao Huang ² and Bowen Cai ³

¹ State Key Laboratory of Information Engineering in Surveying, Mapping and Remote Sensing, Wuhan University, Wuhan 430072, China; guyangu@whu.edu.cn

² Department of Geosciences, University of Arkansas, Fayetteville, AR 72701, USA; xh010@uark.edu

³ School of Remote Sensing and Information Engineering, Wuhan University, Wuhan 430072, China; caibowen@whu.edu.cn

* Correspondence: shaozhenfeng@whu.edu.cn

Abstract: In order to promote the economic development of China's provinces and provide references for the provinces to make effective economic decisions, it is urgent to investigate the trend of province-level economic development. In this study, DMSP/OLS data and NPP/VIIRS data were used to predict economic development. Based on the GDP data of China's provinces from 1992 to 2016 and the nighttime light remote sensing (NTL) data of corresponding years, we forecast GDP via the linear model (LR model), ARIMA model, ARIMAX model, and SARIMA model. Models were verified against the GDP records from 2017 to 2019. The experimental results showed that the involvement of NTL as exogenous variables led to improved GDP prediction.

Keywords: nighttime light remote sensing; gross domestic product (GDP); ARIMA model



Citation: Gu, Y.; Shao, Z.; Huang, X.; Cai, B. GDP Forecasting Model for China's Provinces Using Nighttime Light Remote Sensing Data. *Remote Sens.* **2022**, *14*, 3671. <https://doi.org/10.3390/rs14153671>

Academic Editor: Johannes Puschig

Received: 21 June 2022

Accepted: 27 July 2022

Published: 31 July 2022

Publisher's Note: MDPI stays neutral with regard to jurisdictional claims in published maps and institutional affiliations.



Copyright: © 2022 by the authors. Licensee MDPI, Basel, Switzerland. This article is an open access article distributed under the terms and conditions of the Creative Commons Attribution (CC BY) license (<https://creativecommons.org/licenses/by/4.0/>).

1. Introduction

The rapid development of economies demands better monitoring and forecasting approaches. Gross domestic product (GDP) is widely regarded as one of the major indicators of measuring the sustainable economic development of a country or region [1,2]. It provides a new basis for regional economic development and the formulation of a sustainable development strategy to forecast economic development at various scales [3,4]. GDP data mainly come from surveys from the National Bureau of Statistics or other administrative departments. Despite their authoritativeness, they have intrinsic limitations (e.g., uncertainties introduced by “water injection” [5] and statistical data methods [6]). In order to better forecast GDP, nighttime light (NTL) remote sensing data have gradually emerged as a novel data source. NTL imagery provides a unique opportunity to observe human activities directly from space, which makes many applications possible including mapping urban areas [7], estimating population and urbanization [8,9], and monitoring disasters and conflicts [10]. NTL satellite imagery has increasingly been used by economists as a representative to measure economic activities [11]. The combination of NTL observation data with other data promotes the development of multidisciplinary and interdisciplinary analysis of NTL observations.

Elvidge et al. [12] found a strong correlation between NTL and GDP. In order to study the urban night economy and its relationship with urbanization from the perspective of NTL data, Shao et al. [13] proposed a night light economic index (NLEI). Gonzalez et al. [14] estimated the impact of regional disasters on economic growth in Argentina from 1992 to 2013 using NTL data. Li et al. [15] estimated whether GDP distortion would have an impact on the tax decisions of local state-owned enterprises using NTL data, and the results pointed to a negative correlation between the distorted local GDP and tax avoidance behaviors of local state-owned enterprises. Galimberti et al. [16] evaluated the effectiveness of satellite-based NTL data in predicting country-level GDP growth, and the results proved that NTL

data could improve the accuracy of the model prediction. Sun et al. [17] proposed a deep learning method based on the Contiguous United States (CONUS) time series (2012–2015) county GDP estimation method. Liang et al. [18] studied the spatialization of Ningbo's GDP using NPP/VIIRS NTL data and urban GDP statistical data. Ma et al. [19] explored the spatiotemporal patterns of India's heavy industries using NTL data that spanned from 2012 to 2018. Zhang et al. [20] extracted the Central Yunnan Urban Agglomeration (CYUA) in built-up urban areas through the urban gravity center model and gravity model using the Yunnan Statistical Yearbook and NTL data and further analyzed the connection strength between urban expansion and urban space.

With the continuous development of NTL, it has attracted much attention due to its objectivity and easy access. Its application is not limited to the estimation of social and economic parameters (GDP, regional development, etc.), and many academic societies also use these data to mine applications in different fields [21]. For example, Li et al. [22] used NTL to evaluate the Syrian conflict. Gu et al. [23] studied the relationship between NTL and net primary productivity (NPP). Bayan et al. [24] used NTL to create a map of Eurasian cities, and the accuracy evaluation result was as high as 94%. Weidmann et al. [25] proposed a new measure of local inequality based on NTL emissions data. Peled et al. [26] used NTL data acquired by satellites to divide different built-up areas combined with the building strength of different building materials to obtain the spatial material stock assessments (MSA) in Europe, presenting multi-level aggregation from urban areas to the continent. Oda et al. [27] presented the first man-made CO₂ emission map based on NASA's Black Marble NTL Product Suite (NBM). Straka et al. [28] investigated the effect of tree cover on the relationship between artificial light at night (ALAN) and bats. James et al. [29] investigated the association between residential outdoor night light and breast cancer incidence. Shao et al. [30] proposed a spatially adaptive regression model and realized multi-temporal impervious surface area (ISA) fraction extraction and spatial-temporal analysis with the integrated use of diurnal and nighttime remotely sensed imagery.

Numerous models have been proposed for GDP forecasting. The autoregressive integrated moving average model (ARIMA) model [31] is one of the models widely used to explore the dynamics of time series data. Lim et al. [32] used ARIMA on the longitudinal data, which propounds pragmatic suggestions to help gambling hubs that are destination-dependent to navigate in and recover from crisis such as the COVID-19 pandemic. Kumar et al. [33] adopted X12-ARIMA to adjust the variables and explored the relationship between financial development and economic growth in India. Shuai et al. [34] established ARIMA models based on the GDP data of Shanghai and Shenzhen, respectively, from 1979 to 2018, and the results showed that the model they used could better fit the GDP data series. Zou et al. [35] used the seasonal autoregressive integrated moving average (SARIMA) model to analyze and predict the horizontal displacement of the dam. Taking advantage of the GDP data of Bangladesh from 1960 to 2017, Miah et al. [36] predicted the GDP of Bangladesh in the future using the ARIMA model. Zhu et al. [37] used the ARIMA model to estimate the GDP growth to assess the macroeconomic recovery from natural disasters. By comparing simulated regional GDP values from 2008 to 2014 with actual regional GDP data after the Wenchuan earthquake, they investigated the economic recovery of the worst-hit areas six years later. Ediger et al. [38] used the ARIMA method to estimate the future primary energy demand of Turkey from 2005 to 2020, and the ARIMA forecasting of the total primary energy demand appeared to be more reliable than the summation of the individual forecasts. Ma et al. [39] predicted the GDP of Dongying City from 2017 to 2020 via a constructed time series ARIMA model.

However, existing efforts have tended to focus on provincial and municipal perspectives, and few studies have performed GDP forecasting on the national level. In this study, we aimed to fill this gap by performing GDP forecasting for all Chinese provinces. We obtained NTL data from 1992 to 2016 and long-term GDP series data from the China Statistical Yearbook for model training. GDP data from 2017 to 2019 were used to test the accuracy of the prediction model. The linear regression (LR) model, ARIMA model,

ARIMAX model, and SARIMA model were used to forecast China's province-level GDP. We further evaluated the accuracy of the predicted results and compared the outputs from different models, aiming to reveal their advantages and disadvantages. In addition, we used the model with the best performance to forecast China's economy in 2030. The conceptual and methodological knowledge as well as the results of this study are expected to provide important references for the sustainable development of China's economy.

2. Study Area and Materials

2.1. Study Area

China (Figure 1) is located in the eastern part of Asia. Its administrative region is divided into 23 provinces, five autonomous regions, four municipalities, and two special administrative regions. China covers 9.6 million square km, with the mainland coastline of roughly 18,000 km. It also owns 7600 islands, of which the biggest island covers an area of 35,798 square km. Through planned large-scale construction, China has seen rapid economic development and has quickly become the second largest economy in the world.

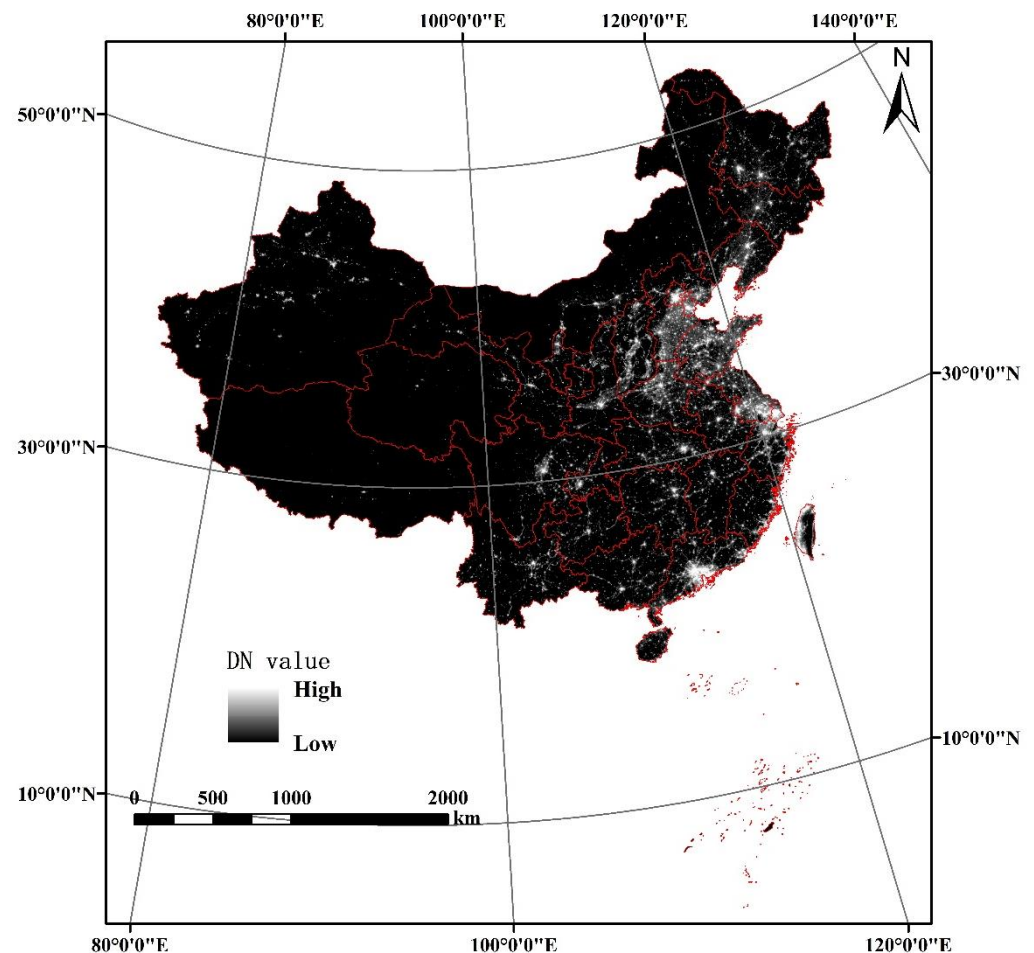


Figure 1. The geographical location of the study area.

2.2. Data Sources

In the 1970s, the United States took the lead in launching the first nighttime light remote sensing satellite (i.e., the Defense Meteorological Satellite Program/Operational Linescan System (DMSP/OLS)). The original intention of DMSP/OLS was to obtain cloud information. Later, the potential of DMSP/OLS in obtaining NTL imagery was explored. Under cloudless conditions at night, NTL remote sensing images can be obtained to reflect human social activities [40]. The National Polar-Orbiting Partnership/Visible Infrared Imaging Radiometer (NPP/VIIRS) was launched in October 2011 with a higher resolution

than the DMSP/OLS imagery. The NTL imagery from NPP/VIIRS, first published in 2012, has widely been used by scholars to monitor and estimate the social and economic indicators given its easy access, objectivity, and strong applicability. Table 1 specifically compares DMSP/OLS and NPP/VIIRS. In this study, we used DMSP/OLS images from 1992 to 2013 and NPP/VIIRS data from 2012 to 2020 to construct a consistent NTL data series at China's provincial level, retrieved from the national environmental information (<https://www.ngdc.noaa.gov>) (accessed on 1 November 2020). In addition, the GDP data used in this study came from the official China Statistical Yearbook.

Table 1. The basic parameters of DMSP/OLS and NPP/VIIRS.

Sensor	DMSP/OLS	Suomi NPP/VIIRS
Archive year	1992–2013	April 2012–
Spatial resolution/m	2700	740
Time resolution/h	12	12
Country	America	America
Data accessibility	Free annual video download, monthly average and daily video to order	Monthly average, daily video free download

3. Methods

The method in this study follows three major steps: (1) NTL calibration; (2) GDP prediction; and (3) accuracy evaluation (Figure 2).

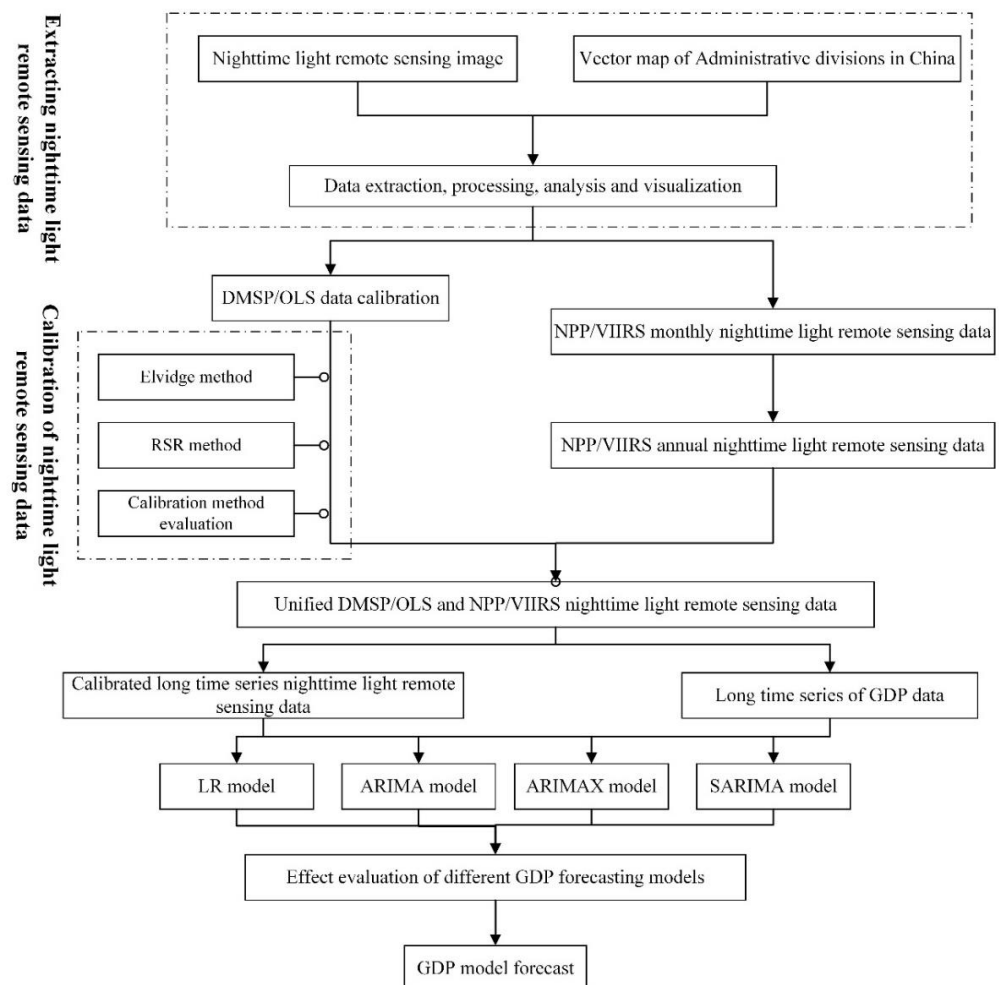


Figure 2. The workflow of the GDP estimation using NTL data.

3.1. Establishing Consistent Long NTL Time Series

DMSP/OLS and NPP/VIIRS, two widely used NTL data, are not comparable, greatly limiting investigations that demand long NTL time series [41]. Therefore, we developed a calibration strategy that included two steps: (1) DMSP/OLS internal calibration; and (2) DMSP/OLS and NPP/VIIRS mutual cross-sensor calibration.

3.1.1. Internal Calibration of DMSP/OLS

Due to the lack of on-board calibration devices and the influence of atmospheric conditions, the image data obtained by DMSP/OLS night-light remote sensing had some limitations such as systematic error and random noise. Thus, internal calibration is necessary.

Widely used DMSP/OLS NTL data calibration methods include polynomial regression (Elvidge) and ridge sampling regression (RSR). Elvidge et al. [12,42] chose Sicily, Italy, as the reference area for DMSP/OLS data calibration and plotted the data of Sicily in the OLS images of all years in the same coordinate system with the data of Sicily in F121999 images. The fitting formula follows:

$$DN_{adj} = C_0 + C_1 \times DN + C_2 \times DN^2 \quad (1)$$

where DN_{adj} is the DN value after calibration of NTL data, and C_0, C_1, C_2 are the polynomial coefficients.

The RSR method was proposed by Zhang et al. [43] based on the assumption that only a small number of NTL pixels changed in a short time. The formula follows:

$$DN_{adj} = a \times DN + b \times DN^2 + c \quad (2)$$

where DN_{adj} is the DN value after the ridge regression analysis of NTL data, and a, b, c are the coefficients of the least square method.

Two additional conditions should be met for data selection (i.e., the calibration error of images taken by different satellites in the same year should be the minimum), and the time series should present a certain level of stableness. Therefore, in order to select the optimal data, the sum of the normalized different index (SNDI) was used to evaluate the calibration error:

$$SNDI = \sum NDI_t \quad (3)$$

$$NDI = \frac{|NTL_{1t} - NTL_{2t}|}{|NTL_{1t} + NTL_{2t}|} \quad (4)$$

where NTL_{1t} and NTL_{2t} represent the NTL values of two images in the same year in the selected area, respectively; NDI represents the normalized different index; $SNDI$ is the sum of NDI .

According to the temporal coverage in Table 2, different satellite data sources at 12 scenes with repeated time points were used to evaluate the effect of the two algorithms.

3.1.2. Cross-Sensor Calibration of DMSP/OLS and NPP/VIIRS

Currently, global-scale NTL data are acquired by two satellite sensors (i.e., DMSP/OLS and NPP/VIIRS), but the data collected by the satellites are not compatible [44]. The NPP/VIIRS NTL data were monthly data from April 2012 to December 2017. We averaged the monthly data to obtain the annual records. Since DMSP/OLS and NPP/VIIRS overlapped in 2012 and 2013, we adopted a relatively simple superposition of the translation method for calibration (STC), which assumed that the NTL observation values of the DMSP/OLS data and NPP/VIIRS data in 2013 were equal, converted the 2013 NPP/VIIRS data to 2013 DMSP/OLS data, and generated the 2013–2019 DMSP/OLS-like NPP/VIIRS data, thus connecting DMSP/OLS and NPP/VIIRS into a longer series of NTL data.

Table 2. The DMSP/OLS satellites and their overlays in the corresponding years.

Year	F10	F12	F14	F15	F16	F18
1992	F101992					
1993	F101993					
1994	F101994	F121994				
1995		F121995				
1996		F121996				
1997		F121997	F141997			
1998		F121998	F141998			
1999		F121999	F141999			
2000			F142000	F152000		
2001			F142001	F152001		
2002			F142002	F152002		
2003			F142003	F152003		
2004				F152004	F162004	
2005				F152005	F162005	
2006				F152006	F162006	
2007				F152007	F162007	
2008					F162008	
2009					F162009	
2010						F182010
2011						F182011
2012						F182012
2013						F182013

3.2. GDP Forecasting Model

In order to reveal the relationship between NTL data and GDP, we adopted four methods (i.e., the LR, ARIMA model, ARIMAX model, and SARIMA model). In this study, we set the seasonal factor as 1. A detailed description of these models is presented below.

3.2.1. Linear Regression (LR) Model

A simple LR model was used to reveal the internal relationship between the NTL data of a long time series and GDP. The LR model is as follows:

$$y_{GDP} = ax_{TNL} + b \quad (5)$$

where x_{TNL} represents the total amount of NTL data and y_{GDP} represents the GDP data.

3.2.2. ARIMA Model

The ARIMA model is built on the basis of autoregression model (AR model) and moving average model (MA model) with the introduction of the difference operation to transform a non-stationary time series into a stationary time series. The ARIMA model is as follows:

$$x_t = c + \sum_{i=0}^p \varphi_i x_{t-i} + \varepsilon_t + \sum_{i=0}^q \theta_i \varepsilon_{t-i} \quad (6)$$

where x_t is the stationary time series data; c is the constant term; φ_i is the coefficient of the autoregressive lag term x_{t-i} ; ε_t is the residual term; θ_i is the coefficient of MA lag term ε_{t-i} ; p is the AR term; and q is the number of MA terms.

3.2.3. ARIMAX Model

Compared with the ARIMA model, the ARIMAX model considers additional exogenous variables, which better solve the problem that unstable variables are prone to false regression and is suitable for multivariate time series data analysis. The mathematical expression of ARIMAX is as follows:

$$y_t = \sum_{j=0}^{\infty} v_j^{(1)} B^j x_t^{(1)} + \sum_{j=0}^{\infty} v_j^{(2)} B^j x_t^{(2)} + \dots + \sum_{j=0}^{\infty} v_j^{(k)} B^j x_t^{(k)} + \frac{\theta(B)}{\varphi(B)} \alpha_t \quad (7)$$

where $(B) = 1 - \theta_1 B - \dots - \theta_q B^q$; $\varphi(B) = 1 - \varphi_1 B - \dots - \varphi_p B^p$ is called the transfer function model; $x_t^{(j)}$ is the input factor; and y_t is the output factor.

3.2.4. SARIMA Model

In time series analysis, certain time sequences can contain notable cyclical changes. If the tendency fails to follow a linear change, ARIMA often falls short in deriving its changing dynamics. Thus, SARIMA, the seasonal version of the ARIMA model, can be used. The general expression of a SARIMA model is as follows:

$$x_t = \Delta^d \Delta_s^D y_t \quad (8)$$

$$(1 - \varnothing_1 L - \dots - \varnothing_p L^p) (1 - \alpha_1 L^s - \dots - \alpha_p L^{ps}) (\Delta^d \Delta_s^D y_t) = (1 + \theta_1 \dots + \theta_q L^q) (1 \beta_1 L^s \dots \beta_Q \beta^{Qs}) u_t \quad (9)$$

where Δ , Δ_s represent the seasonal differences of the non-seasonal and S-phase, respectively; d and D represent the non-seasonal and seasonal differences, respectively; p, P, q, Q represent the maximum lag order of non-seasonal, seasonal, AR, and MA operators, respectively.

3.3. Accuracy Evaluation

In order to explore the advantages and disadvantages of the above four GDP forecasting models and seek the best GDP forecasting model, the following formula was used to evaluate the accuracy of the GDP forecasting models:

$$r = \frac{|GDP_{pred} - GDP_{real}|}{GDP_{real}} \times 100\% \quad (10)$$

where GDP_{pred} represents the data obtained through the GDP prediction model and GDP_{real} represents the official GDP data from China's Statistical Yearbook.

4. Results

4.1. The Calibration of the NTL

We first performed an internal calibration on the DMSP/OLS data. The calibration results of the method adopted from Elvidge et al. [12,42] and the RSR method adopted from Zhang et al. [43] were obtained (Figure 3). Compared with the original uncalibrated DMSP/OLS data (Figure 3a), the calibrated DMSP/OLS NTL time series presented considerably smoother patterns.

According to the standard errors calculated by overlapping satellites, the calibration errors of the NTL images of different satellites in the same year based on different calibration methods are shown in Table 3. The SNE_{raw} of the uncalibrated DMSP/OLS data was 2.033. In comparison, the $SNE_{Elvidge}$ was 1.132, while the calculated SNE_{RSR} was 1.108. The above results suggest that both calibration methods significantly reduced the errors compared with the uncalibrated DMSP/OLS data, and the RSR calibration method outperformed the Elvidge method.

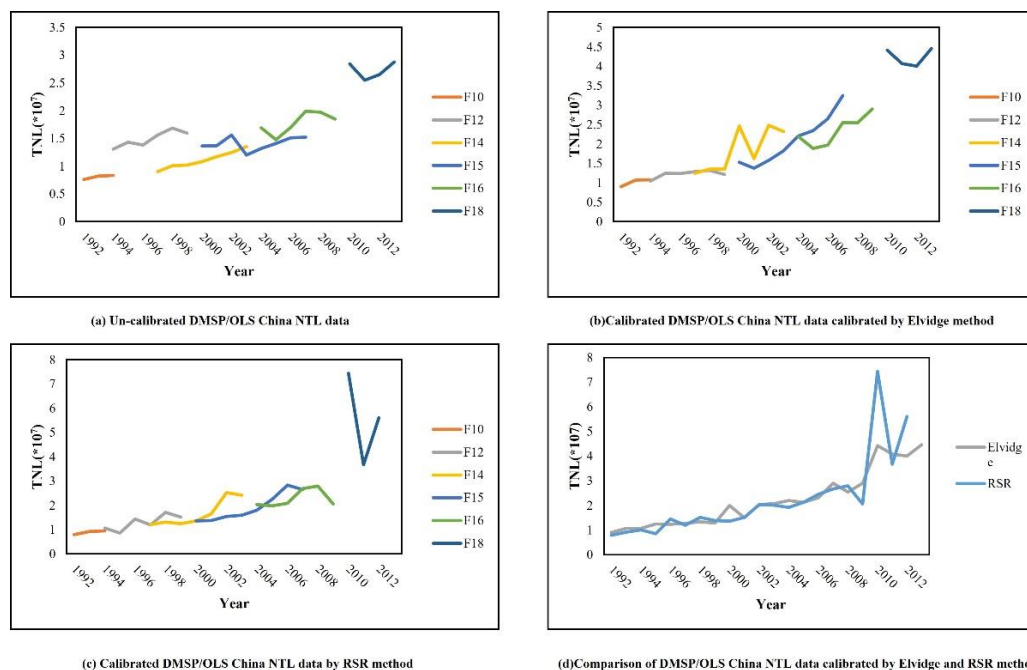


Figure 3. The DMSP/OLS NTL data before and after the calibrations using two different methods. ((a) Un-calibrated DMSP/OLS NTL data, (b) Calibrated NTL data calibrated by Elvidge method, (c) Calibrated NTL data by RSR method, (d) Comparison of DMSP/OLS NTL data calibrated by Elvidge and RSR method).

Table 3. The calibration errors of the NTL images based on different methods.

Year	Satellite 1	Satellite 2	Raw	Elvidge	RSR		
1994	F10	F12	0.023	0.015	0.052		
1997	F12	F14	0.532	0.017	0.008		
1998	F12	F14	0.089	0.012	0.129		
1999			F12	F14	0.077	0.054	0.099
2000			F14	F15	0.238	0.234	0.002
2001			F14	F15	0.361	0.084	0.088
2002			F14	F15	0.241	0.221	0.242
2003			F14	F15	0.086	0.118	0.206
2004			F15	F16	0.006	0.003	0.059
2005			F15	F16	0.079	0.108	0.064
2006			F15	F16	0.149	0.145	0.151
2007			F15	F16	0.150	0.119	0.008
					2.033	1.132	1.108

Figure 4 presents the calibration coefficients of the RSR method with F152000 as the reference image. We noted that records from the F18 satellite greatly deviated from the other records. Therefore, it can be inferred that the RSR method perform poorly on images from the F18 satellite. Thus, we used the RSR method to calibrate the NTL data from 1992 to 2007 and the Elvidge method to calibrate the NTL data from 2008 to 2013. Finally, continuous calibrated NTL data that spanned from 1992 to 2019 after calibration was obtained (Figures 5 and 6). From Figure 5, we can observe that, in general, Eastern China is notably brighter than Western China, with urban agglomeration in the Yangtze River Delta presenting the highest light intensity. From 1992 to 2019, many rural areas in China, especially in the central regions, have been developed, as evidenced by their increasing amount of light intensity. From Figure 6, we can see that the unified NTL data of the long time series showed good stable growth characteristics. Thus, the accuracy and reliability of our calibration strategy were further verified.

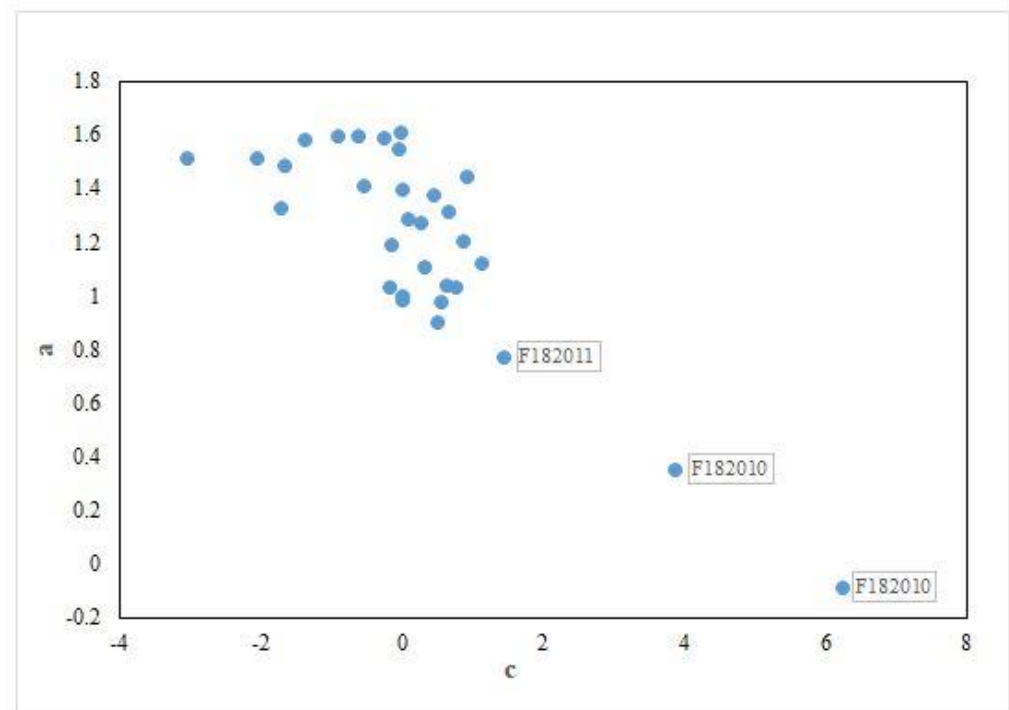


Figure 4. The calibration coefficients of the RSR method with F152000 as the reference image.

4.2. NTL–GDP Relationship and Model Evaluation

Based on the above four models, the NTL data from 1992 to 2016 were taken as the training set, while the NTL data from 2017 to 2019 were used to evaluate the models' performance, serving as the verification set.

Through the simple LR model (Figure 7), it can be seen that there was a strong positive correlation between the NTL intensity and GDP during the 25-year span (1992–2016). Despite the high R^2 of the GDP prediction model based on LR, the GDP prediction accuracy had an average error of 19.26%.

To predict GDP in the years 2017, 2018, and 2019 using the NTL data from 1992 to 2016, we tested three additional models (i.e., classic ARIMA, seasonal variable SARIMA, and exogenous ARIMAX). The predicted results in selected Chinese provinces are presented in Figures 8 and 9. The average errors based on the ARIMA model, SARIMA model, and ARIMAX models were 8.44, 6.98, and 4.51%, respectively. The above results suggest that compared with the LR model, the overall accuracy of the other three models was improved, and ARIMAX model had the best performance among the three models. As an exogenous variable, NTL can play a good correction role in the GDP prediction model with the minimum error, thus proving once again that NTL plays an important role in the exploration of urban economic development and the analysis and prediction of urban GDP changes by NTL.

Figure 10 presents the spatial distribution of errors at China's provincial level. We observed that certain provinces presented considerably larger errors than others. The reasons may be as follows. (1) The GDP data themselves have a non-trend fluctuation, while NTL resulting from urbanization continues to increase. For example, Liaoning (with a large error in all four GDP forecasting methods) had a large fluctuation in GDP data, with a clear upward trend from 1992 to 2015 and a sudden drop in 2016. Such GDP fluctuations failed to be captured by the models, as non-trend fluctuations pose great challenges for all forecasting models. (2) The NTL data themselves contain a certain level of uncertainty. From Figure 10, we notice that, in general, that the GDP prediction error of southern provinces was smaller than that of northern provinces, which may be related to the errors of the NTL data themselves. In addition, we found periodic changes in abnormal data

when processing the experimental data. (3) NTL fails to represent GDP in a comprehensive manner. Compared to the South, North China has more extensive land urbanization. In certain places, extensive impervious surfaces and a large number of artificial objects could correspond to high GDP, but they failed to be captured by NTL intensity, leading to the severe underestimation of GDP.

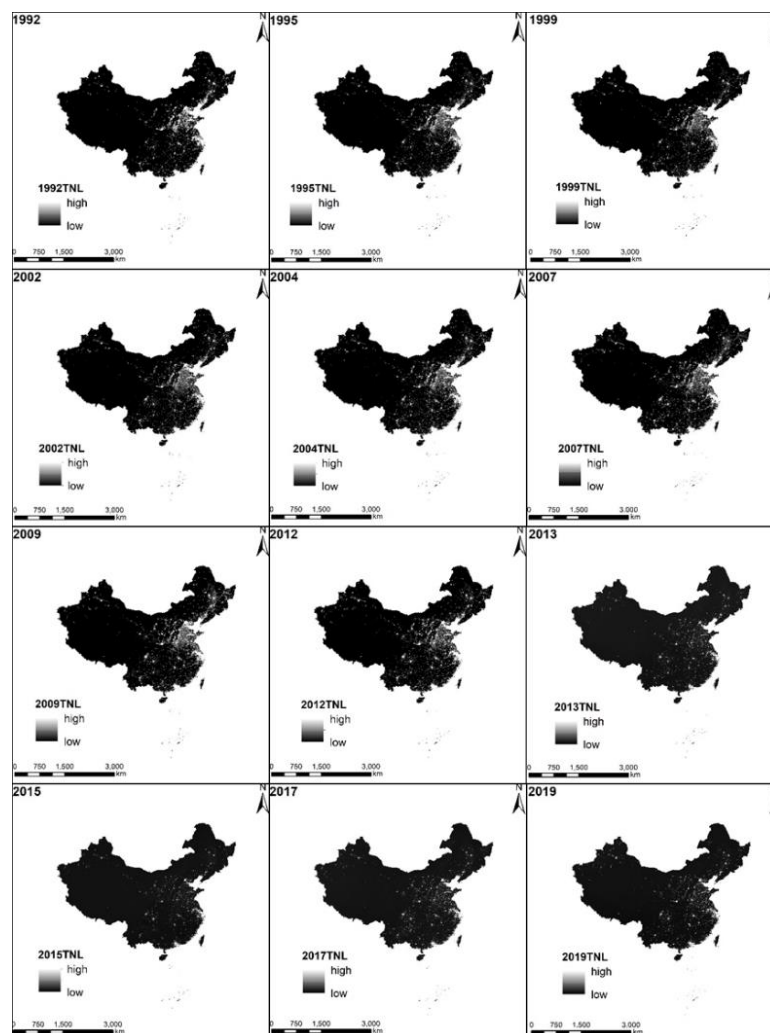


Figure 5. The calibrated NTL remote sensing images in China from 1992 to 2019.

4.3. GDP Forecast in 2030

Using the ARIMAX model, a model with the smallest error in the verification dataset, we forecast the GDP of China's provinces (except Taiwan). The forecast results are presented in Figure 11 and Table 4. The results show that by 2030, the Chinese economy will be more than 1.6 quintillion yuan, with provinces that include Tianjin, Guizhou, and Xizang having a higher predicted growth while provinces that include Shanxi and Liaoning having a small predicted growth.

From the perspective of spatial variation, the economic aggregate of Jiangsu and Guangdong is expected to continue to lead all other provinces in China, both exceeding 190,000 trillion yuan, while the economic aggregate of Xizang and Qinghai will lag behind, both less than 5000 trillion yuan. Such a result indicates unbalanced economic development in China. The economic aggregate of the South has higher GDP than that of the North, while the economic development of the East is stronger than that of the West. In terms of provinces, the economic aggregate of Guangdong and Jiangsu is notably stronger than that of other provinces. China's future economic policy formulation can be further carried out

in the direction of addressing the unbalanced regional economic development, aiming for a more sustainable and even development.



Figure 6. The statistical value of the calibrated NTL data in selected Chinese provinces from 1992 to 2019.

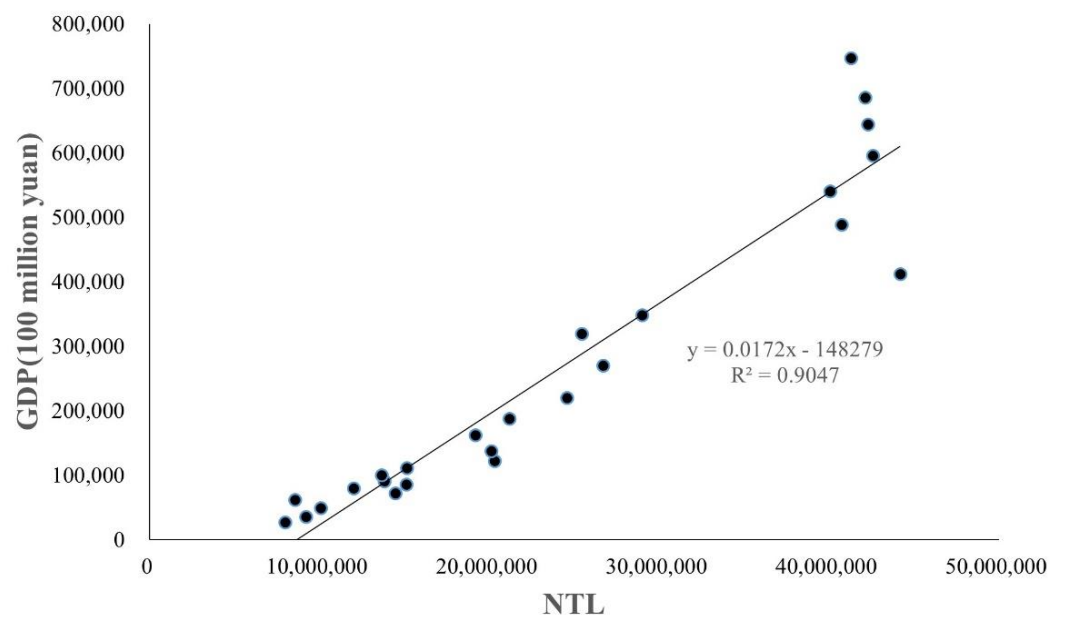


Figure 7. The NTL data and GDP in China from 1992 to 2016 (LR results).

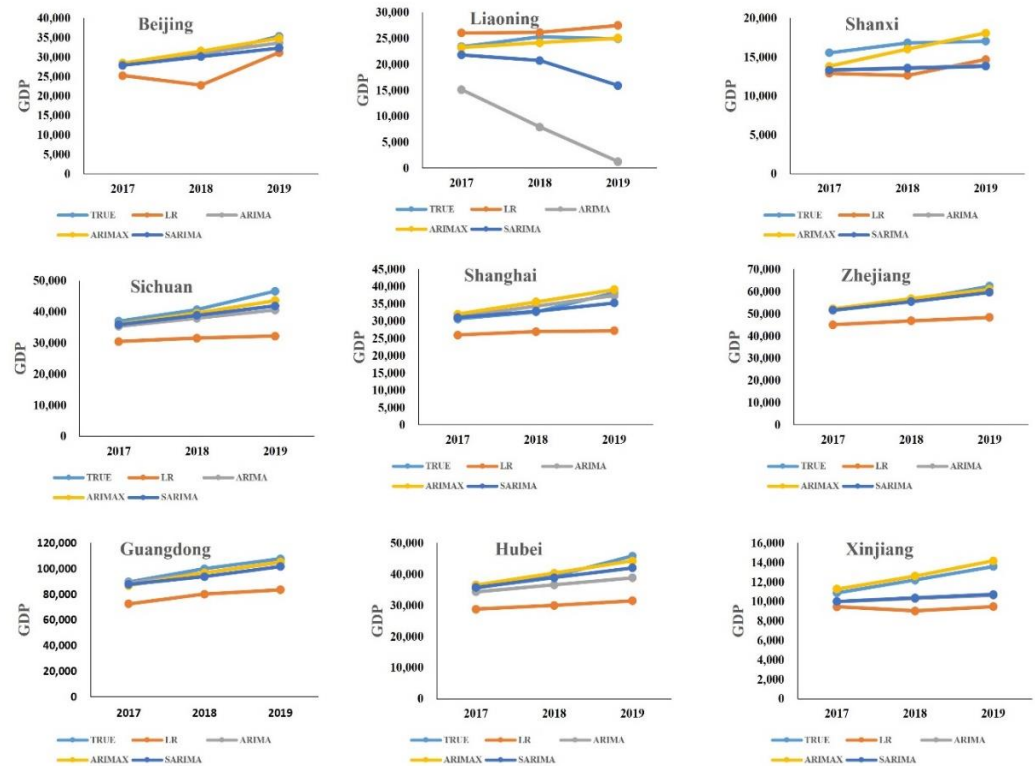


Figure 8. The GDP predicted by different models in selected Chinese provinces.

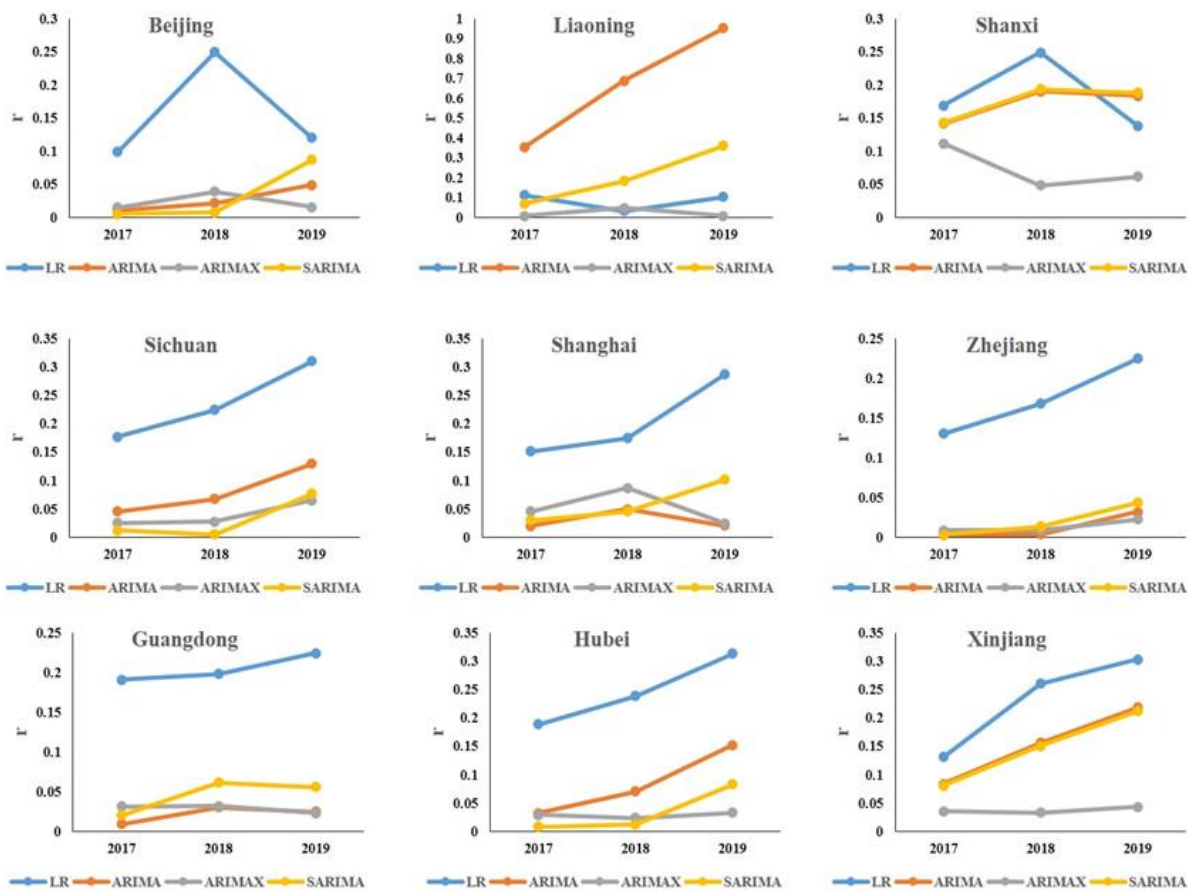


Figure 9. The r of different GDP forecasting models in selected Chinese provinces.

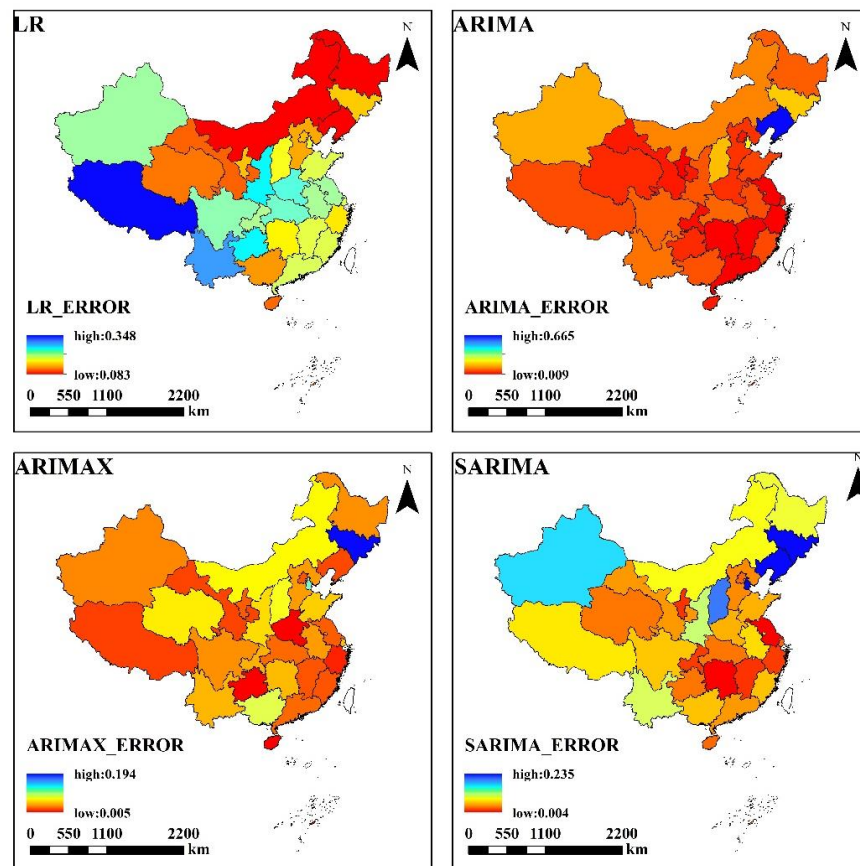


Figure 10. The comparison of the average error of the different GDP forecast models in China.

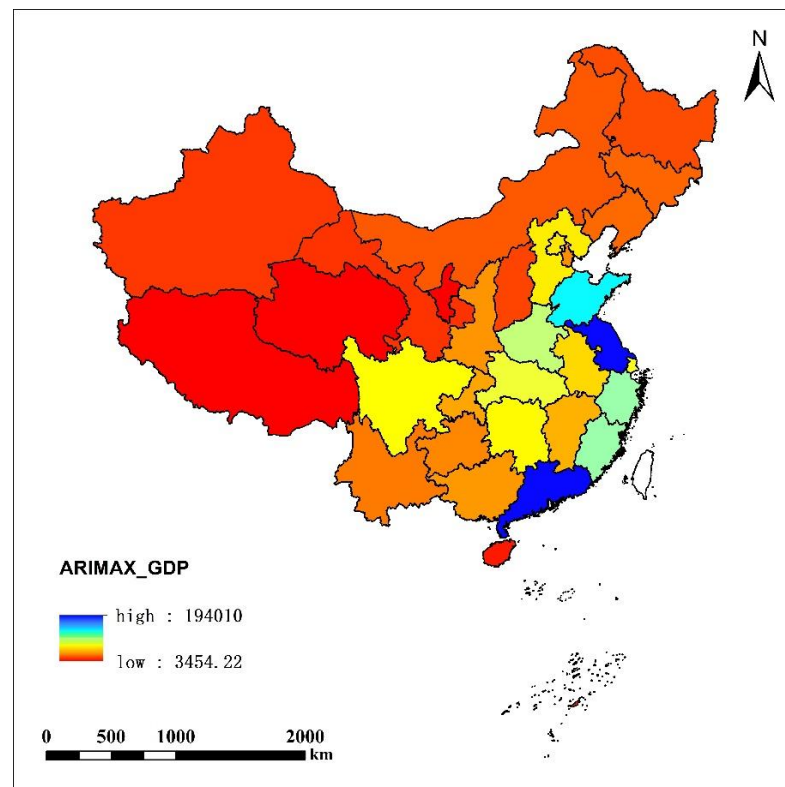


Figure 11. The 2030 GDP forecast of Chinese provinces (except Taiwan) using the ARIMAX model.

Table 4. A comparison of the GDP forecast of Chinese provinces in 2030 using the ARIMAX model.

Province	Year	Trillion Yuan	Province	Year	Trillion Yuan	Province	Year	Trillion Yuan
Beijing		62,832.69	Tianjin		36,746.19	Hebei		63,771.21
Shanxi		19,321.30	Neimenggu		22,280.36	Liaoning		26,416.12
Jilin		24,768.18	Heilongjiang		19,619.97	Shanghai		71,024.35
Jiangsu		194,010.35	Zhejiang		108,359.54	Anhui		58,035.48
Fujian		68,441.22	Jiangxi		46,614.7	Shandong		13,3058.04
Henan		95,018.14	Hubei		76,278.04	Hunan		68,639.61
Guangdong		193,447.95	Guangxi		39,520.92	Hainan		8959.36
Chongqing		43,340.22	Sichuan		69,464.10	Guizhou		35,046.67
Yunnan		31,157.92	Xizang		3454.22	Shaanxi		38,687.81
Gansu		12,941.07	Qinghai		4720.20	Ningxia		6764.07
Xinjiang		14,198.30						

5. Discussion

The development of NTL data has provided a new common data source for the spatialization of social and economic data, with strong application and analysis ability. This section will further discuss the spatio-temporal changes and limitations, respectively.

5.1. Time Change of GDP

NTL can directly reflect the differences in human activities and has a wide application space in economic analysis. It can be seen from Figures 5 and 11 that all provinces in China are in a stage of steady growth, which is of great importance to the 14th National Congress of the Communist Party of China, which proposed combining the basic socialist system with the market economy to establish a socialist market economic system. The national economy is growing at a high speed, and production, construction, distribution, and opening-up are developing in an all-round way, and people's living standards are being further improved. Judging from the GDP forecasts, China is on track to achieve this goal.

5.2. Spatial Variation of GDP

The NTL reflects the human activities in a region at night. The NTL brightness in developed cities is significantly higher than that in small cities. Therefore, NTL data can reflect the social and economic development of a region to a certain extent, and better show the consistency of urban economic development. After the reform and opening-up policy since 1978, the Chinese government has embarked on a regional economic development strategy for a large change, from an unbalanced development strategy to a balanced development strategy, with priority given to the development of coastal areas. The development and the open policy tilt toward coastal regions has obviously made coastal areas develop more rapidly, thus quickly widening the economic development gap between the coast and inland. The eastern region is obviously stronger than the western region. After the reform and opening up, the "strong north and weak south" has rapidly changed to the "strong south and weak north", and there is a big development gap between provinces. To address the problem of unbalanced regional development, China has successively implemented the strategy of the large-scale development of the Western region, the strategy of revitalizing the old industrial base in Northeast China, and the strategy of promoting the rise of the Central region.

5.3. Limitation Analysis

Although there is a strong relationship between the NTL data and human society economic activity based on the NTL built GDP model, which have important research value, this study does not take into account the NTL "fraud" [45], the global crisis (such as COVID-19 pandemic [46,47], the Russo-Ukrainian War), and so on. In addition, the

NTL field also has many problems, for example, the night light photometric units have not been clearly defined, the different platform and sensor lights at night time sequence consistency problem due to the angle of the atmosphere and surface optical properties, the daily variation and seasonal variation caused by the night lights, and the uncertainty of measurement error [48]. At the same time, based on the optical wavelengths of observation at night, there are many challenges such as artificial light, vegetation changes, the change of the street layout and building height, so night lights will change accordingly [49]. Due to the light emitting diode (LED) [50] technology to the development of the cause of a “lighting revolution”, the world is in transition to the LED, so lamp remote sensing has a great influence on NTL. Therefore, from the perspective of NTL, the quantitative refinement study of economic development is the focus of future research.

6. Conclusions

Based on the historical GDP data from 1992 to 2016 and the calibrated annual NTL data from DMSP/OLS and NPP/VIIRS, we tested the GDP forecasting capability of models that included the LR model, ARIMA model, ARIMAX model, and SARIMA model. Model performances were evaluated by deriving the GDP values in 2017, 2018, and 2019 by using the NTL data from 1992 to 2016. After a comparison with the original GDP data, the results showed that the ARIMAX model achieved the best prediction result. Our study suggests that the NTL intensity was highly correlated with the GDP values, and the involvement of NTL benefits the GDP prediction models. We further predicted China’s GDP in 2030 using the ARIMAX model, and the results showed that China’s economy will continue to grow, but the growth rate will greatly differ in different provinces. Such a result points to the necessity of establishing regional development plans that address the uneven development. To solve the problem of unbalanced regional development is a long-term process, which must be based on the long-term and rationally planned.

Author Contributions: Conceptualization, Y.G. and B.C.; Methodology, Y.G.; Software, Y.G.; Validation, Y.G. and B.C.; Formal analysis, Y.G.; Resources, Z.S.; Data curation, Z.S.; Writing—original draft preparation, Y.G. and B.C.; Writing—review and editing, B.C., Z.S., and X.H.; Supervision, X.H.; Project administration, Z.S.; All authors have read and agreed to the published version of the manuscript.

Funding: This work was supported by the National Natural Science Foundation of China with grant number 42090012; the National Key Research and Development Program of China with grant number 2018YFB2100501; and the National Natural Science Foundation of China with grant numbers 41771452 and 41771454.

Data Availability Statement: No applicable.

Acknowledgments: We are grateful to those who participated in the data processing and manuscript revisions.

Conflicts of Interest: The authors declare no conflict of interest.

References

1. Chen, X.; Nordhaus, W. VIIRS Nighttime Lights in the Estimation of Cross-Sectional and Time-Series GDP. *Remote Sens.* **2019**, *11*, 1057. [[CrossRef](#)]
2. Cai, B.; Shao, Z.; Fang, S.; Huang, X. Quantifying Dynamic Coupling Coordination Degree of Human–Environmental Interactions during Urban–Rural Land Transitions of China. *Land* **2022**, *11*, 935. [[CrossRef](#)]
3. Li, Z.; Jiao, L.; Zhang, B.; Xu, G.; Liu, J. Understanding the pattern and mechanism of spatial concentration of urban land use, population and economic activities: A case study in Wuhan, China. *Geo-Spat. Inf. Sci.* **2021**, *24*, 678–694. [[CrossRef](#)]
4. Zhuang, Q.; Shao, Z.; Li, D.; Huang, X.; Cai, B.; Altan, O.; Wu, S. Unequal weakening of urbanization and soil salinization on vegetation production capacity. *Geoderma* **2022**, *411*, 115712. [[CrossRef](#)]
5. Marc, F.; Philippe, M. The news of the death of welfare economics is greatly exaggerated. *Soc. Choice Welf.* **2005**, *25*, 381–418. [[CrossRef](#)]
6. Huh, H.; Chung, M. A method to allocate GDP statistical discrepancy. *Appl. Econ. Lett.* **2006**, *13*, 587–591. [[CrossRef](#)]

7. Zhang, X.; Guo, S.; Guan, Y.; Cai, D.; Zhang, C.; Fraedrich, K.; Xiao, H.; Tian, Z. Urbanization and Spillover Effect for Three Megaregions in China: Evidence from DMS/OLS Nighttime Lights. *Remote Sens.* **2018**, *10*, 1888. [[CrossRef](#)]
8. Xu, P.; Jin, P.; Yang, Y.; Wang, Q.; Bagan, H. Evaluating Urbanization and Spatial-Temporal Pattern Using the DMS/OLS Nighttime Light Data: A Case Study in Zhejiang Province. *Math. Probl. Eng.* **2016**, *2016*, 9850890. [[CrossRef](#)]
9. Cai, B.; Shao, Z.; Fang, S.; Huang, X.; Huq, M.E.; Tang, Y.; Li, Y.; Zhuang, Q. Finer-scale spatiotemporal coupling coordination model between socioeconomic activity and eco-environment: A case study of Beijing, China. *Ecol. Indic.* **2021**, *131*, 108165. [[CrossRef](#)]
10. Li, X.; Liu, S.; Jendryke, M.; Li, D.; Wu, C. Night-Time Light Dynamics during the Iraqi Civil War. *Remote Sens.* **2018**, *10*, 858. [[CrossRef](#)]
11. Shao, Z.; Tang, Y.; Huang, X.; Li, D. Monitoring Work Resumption of Wuhan in the COVID-19 Epidemic Using Daily Nighttime Light. *Photogramm. Eng. Remote Sens.* **2021**, *87*, 197–206. [[CrossRef](#)]
12. Elvidge, C.; Ziskin, D.; Baugh, K.; Tuttle, B.; Ghosh, T.; Pack, D.; Erwin, E.; Zhizhin, M. A Fifteen Year Record of Global Natural Gas Flaring Derived from Satellite Data. *Energies* **2009**, *2*, 595–622. [[CrossRef](#)]
13. Fu, H.; Shao, Z.; Fu, P.; Cheng, Q.; Yu, B.; Thenkabail, P. The Dynamic Analysis between Urban Nighttime Economy and Urbanization Using the DMS/OLS Nighttime Light Data in China from 1992 to 2012. *Remote Sens.* **2017**, *9*, 416. [[CrossRef](#)]
14. Gonzales, F.; London, S.; Santos, M. Disasters and economic growth: Evidence for Argentina. *Clim. Dev.* **2021**, *13*, 932–943. [[CrossRef](#)]
15. Li, X.; Cai, G.; Luo, D. GDP distortion and tax avoidance in local SOEs: Evidence from China. *Int. Rev. Econ. Financ.* **2020**, *69*, 582–598. [[CrossRef](#)]
16. Galimberti, J. Forecasting GDP Growth from Outer Space. *Oxf. Bull. Econ. Stat.* **2020**, *82*, 697–722. [[CrossRef](#)]
17. Sun, J.; Di, L.; Sun, Z.; Wang, J.; Wu, Y. Estimation of GDP Using Deep Learning with NPP-VIIRS Imagery and Land Cover Data at the County Level in CONUS. *IEEE J. Sel. Top. Appl. Earth Obs. Remote Sens.* **2020**, *13*, 1400–1415. [[CrossRef](#)]
18. Liang, H.; Guo, Z.; Wu, J.; Chen, Z. GDP spatialization in Ningbo City based on NPP/VIIRS night-time light and auxiliary data using random forest regression. *Adv. Space Res.* **2020**, *65*, 481–493. [[CrossRef](#)]
19. Ma, C.; Niu, Y.; Ma, Y.; Chen, F.; Yang, J.; Liu, J. Assessing the Distribution of Heavy Industrial Heat Sources in India between 2012 and 2018. *ISPRS Int. J. Geo-Inf.* **2020**, *8*, 568. [[CrossRef](#)]
20. Zhang, E.; Feng, H.; Peng, S.; Gary, A. Measurement of Urban Expansion and Spatial Correlation of Central Yunnan Urban Agglomeration Using Nighttime Light Data. *Math. Probl. Eng.* **2021**, *2021*, 8898468. [[CrossRef](#)]
21. Levin, N.; Kyba, C.; Zhang, Q.; Miguel, A.; Román, M.; Li, X.; Portnov, B.; Molthan, A.; Jechow, A.; Miller, S.; et al. Remote sensing of night lights: A review and an outlook for the future. *Remote Sens. Environ.* **2020**, *237*, 111443. [[CrossRef](#)]
22. Li, X.; Li, D. Can night-time light images play a role in evaluating the Syrian Crisis? *Int. J. Remote Sens.* **2014**, *35*, 6648–6661. [[CrossRef](#)]
23. Gu, Y.; Shao, Z.; Huang, X.; Fu, Y.; Gao, J.; Fan, Y. Assessing the Impact of Land Use Changes on Net Primary Productivity in Wuhan, China. *Photogramm. Eng. Remote Sens.* **2022**, *88*, 189–197. [[CrossRef](#)]
24. Bayan, A.; Ryutaro, T.; Dong, X.; Nguyen, T.; Ahmad, A.; Bai, X. New urban map of Eurasia using MODIS and multi-source geospatial data. *Geo-Spat. Inf. Sci.* **2017**, *20*, 29–38. [[CrossRef](#)]
25. Weidmann, N.; Theunissen, G. Estimating Local Inequality from Nighttime Lights. *Remote Sens.* **2021**, *13*, 4642. [[CrossRef](#)]
26. Peled, Y.; Fishman, T. Estimation and mapping of the material stocks of buildings of Europe: A novel nighttime lights-based approach. *Resour. Conserv. Recycl.* **2021**, *169*, 105509. [[CrossRef](#)]
27. Oda, T.; Román, M.; Wang, Z.; Stokes, E.; Sun, Q.; Shrestha, R.; Feng, S.; Lauvaux, T.; Bun, R.; Maksyutov, S.; et al. US Cities in the Dark: Mapping Man-Made Carbon Dioxide Emissions Over the Contiguous US Using NASA's Black Marble Nighttime Lights Product. In *Urban Remote Sensing: Monitoring, Synthesis, and Modeling in the Urban Environment*, 2nd ed.; Yang, X., Ed.; Wuhan University: Wuhan, China, 2021; pp. 337–367. [[CrossRef](#)]
28. Straka, T.; Wolf, M.; Gras, P.; Buchholz, S.; Voigt, C. Tree cover mediates the effect of artificial light on urban bats. *Front. Ecol. Evol.* **2019**, *7*, 91. [[CrossRef](#)]
29. James, P.; Bertrand, K.; Hart, J.; Schernhammer, E.; Tamimi, R.; Laden, F. Outdoor light at night and breast cancer incidence in the nurses' health study II. *Environ. Health Perspect.* **2017**, *125*, 087010. [[CrossRef](#)]
30. Shao, Z.; Chong, L. The Integrated Use of DMS/OLS Nighttime Light and MODIS Data for Monitoring Large-Scale Impervious Surface Dynamics: A Case Study in the Yangtze River Delta. *Remote Sens.* **2014**, *6*, 9359–9378. [[CrossRef](#)]
31. Ledolter, J.; Box, G. Conditions for the optimality of exponential smoothing forecast procedures. *Springer Nat. J.* **1978**, *25*, 77–93. [[CrossRef](#)]
32. Lim, W.; To, W. The economic impact of a global pandemic on the tourism economy: The case of COVID-19 and Macao's destination- and gambling-dependent economy. *Curr. Issues Tour.* **2021**, *25*, 1258–1269. [[CrossRef](#)]
33. Kumar, K.; Paramanik, R. Nexus between Indian Economic Growth and Financial Development: A Non-Linear ARDL Approach. *J. Asian Financ. Econ. Bus.* **2020**, *7*, 109–116. [[CrossRef](#)]
34. Shuai, Y.; Zhou, Z. GDP Analysis and Comparison in Coastal Cities Based on Time Series Analysis. *J. Coast. Res.* **2019**, *98*, 402–406. [[CrossRef](#)]
35. Zou, J.; Bui, K.; Xiao, Y.; Doan, C. Dam deformation analysis based on BPNN merging models. *Geo-Spat. Inf. Sci.* **2018**, *21*, 149–157. [[CrossRef](#)]

36. Miah, M.; Tabassum, M.; Rana, M. Modelling and Forecasting of GDP in Bangladesh: An ARIMA Approach. *J. Mech. Contin. Math. Sci.* **2019**, *14*, 150–166. [[CrossRef](#)]
37. Zhu, Y.; Wang, Y.; Liu, T.; Sui, Q. Assessing macroeconomic recovery after a natural hazard based on ARIMA—A case study of the 2008 Wenchuan earthquake in China. *Nat. Hazards* **2018**, *91*, 1025–1038. [[CrossRef](#)]
38. Ediger, V.; Akar, S. ARIMA forecasting of primary energy demand by fuel in Turkey. *Energy Policy* **2007**, *35*, 1701–1708. [[CrossRef](#)]
39. Ma, L.; Hu, C.; Lin, R.; Han, Y. ARIMA model forecast based on EViews software. In Proceedings of the International Conference on Air Pollution and Environmental Engineering 2018, Hong Kong, China, 26–28 October 2018. [[CrossRef](#)]
40. Zhao, N.; Cao, G.; Zhang, W.; Samson, E.; Chen, Y. Remote sensing and social sensing for socioeconomic systems: A comparison study between nighttime lights and location-based social media at the 500 m spatial resolution. *Int. J. Appl. Earth Obs. Geoinf.* **2020**, *87*, 102058. [[CrossRef](#)]
41. Dong, K.; Li, X.; Cao, H.; Tong, Z. Intercalibration Between Night-Time DMSP/OLS Radiance Calibrated Images and NPP/VIIRS Images Using Stable Pixels. *IEEE J. Sel. Top. Appl. Earth Obs. Remote Sens.* **2021**, *14*, 8838–8848. [[CrossRef](#)]
42. Elvidge, C.; Hsu, F.; Baugh, K.; Ghosh, T.; Weng, Q. National Trends in Satellite-Observed Lighting: 1992–2012. *Remote Sens. Appl. Ser.* **2014**, *23*, 97–118. [[CrossRef](#)]
43. Zhang, Q.; Pandey, B.; Seto, K. A robust method to generate a consistent time series from DMSP/OLS nighttime light data. *IEEE Trans. Geosci. Remote Sens.* **2016**, *54*, 5821–5831. [[CrossRef](#)]
44. Zheng, Q.; Weng, Q.; Wang, K. Developing a new cross-sensor calibration model for DMSP-OLS and Suomi-NPP VIIRS night-light imageries. *ISPRS J. Photogramm. Remote Sens.* **2019**, *153*, 36–47. [[CrossRef](#)]
45. Green, J.; Perkins, C.; Steinbach, R.; Edwards, P. Reduced street lighting at night and health: A rapid appraisal of public views in England and Wales. *Health Place* **2015**, *34*, 171–180. [[CrossRef](#)] [[PubMed](#)]
46. Altan, O.; Dowman, I. The changing world under the corona virus threat—from human needs to SDGs and what next? *Geo-Spat. Inf. Sci.* **2021**, *24*, 50–57. [[CrossRef](#)]
47. Griffith, D.; Li, B. Spatial-temporal modeling of initial COVID-19 diffusion: The cases of the Chinese Mainland and Conterminous United States. *Geo-Spat. Inf. Sci.* **2021**, *24*, 340–362. [[CrossRef](#)]
48. Román, M.; Wang, Z.; Sun, Q.; Kalb, V.; Miler, S.; Molthan, A.; Schultz, L.; Bell, J.; Stokes, E.; Pandey, B.; et al. NASA’s Black Marble nighttime lights product suite. *Remote Sens. Environ.* **2018**, *210*, 113–143. [[CrossRef](#)]
49. Kyba, C.; Garz, S.; Kuechly, H.; De Miguel, S.; Zamorano, J.; Fischer, J.; Hölker, F. High-resolution imagery of earth at night: New sources, opportunities and challenges. *Remote Sens.* **2015**, *7*, 1–23. [[CrossRef](#)]
50. Sánchez de Miguel, A.; Aubé, M.; Zamorano, J.; Kocifaj, M.; Roby, J.; Tapia, C. Sky Quality Meter measurements in a colour-changing world. *Mon. Not. R. Astron. Soc.* **2017**, *467*, 2966–2979. [[CrossRef](#)]